Earthq Eng & Eng Vib (2011) 10: 187-193 **DOI**: 10.1007/s11803-011-0057-1

Behavior of large post-liquefaction deformation in saturated Nanjing fine sand

Pan Hua[1†], Chen Guoxing[1,2‡], Liu Hanlong[2‡] and Wang Binghui[1†]

1. *Institute of Geotechnical Engineering, Nanjing University of Technology, Nanjing 210009, China*

2. *Geotechnical Research Institute, Hohai University, Nanjing 210098, China*

Abstract: Laboratory tests on the large post-liquefaction deformation of saturated Nanjing fine sand were performed by using a hollow cylinder apparatus. The stress-strain responses and the characteristics of excess pore water pressure after liquefaction were studied. It was found that the relationship between deviatoric stress and axial strain presented a sigmoid curve, and there was a good linearity relationship between normalized pore water pressure and deviatoric stress. On this basis, a constitutive model of stress-strain responses and a dissipation model of excess pore water pressure were established. It was found that the results predicted by the two models were in good agreement with the experimental data. The influence of relative densities and confining pressure on the characteristics of liquefied soil were studied. The results showed the relative densities and initial effective confining pressure all had an important influence on the stress-strain responses of liquefied saturated Nanjing fine sand. However, the dissipation model of excess pore water pressure after liquefaction was only affected by the confining pressure.

Keywords: saturated Nanjing fine sand; large post-liquefaction deformation; constitutive model; dissipation model of excess pore water pressure

1 Introduction

Stability and deformation are two major themes in geotechnical engineering. However, deformation, considered as a main reason for earthquake damage, is a key issue in soil dynamics research, which was confirmed following surveys of previous earthquake damage (Hamada *et al*., 1987; Tohno and Shamoto, 1985; Tohno and Shamoto, 1986). Damage induced by liquefaction of soil is almost always related to large deformations (Hamada *et al.*, 1996; Shamoto *et al.*, 1997), thus the prediction of large post-liquefaction deformation has a very important engineering significance.

Some researchers have focused on a prediction method for large post-liquefaction deformation. Hamada *et al*. (1986), Tokimatsu and Seed (1987), Ishihara and Yoshimine (1992) , Towhata *et al*. (1992), Bartlett and Youd (1995) established prediction formula of large post-liquefaction deformation based on experimental data and seismic survey results. Yasuda *et al*. (1995) proposed a double line model of stress-strain relationship of sand after liquefaction based on laboratory tests. Liu *et al*. (2002) conducted a series of triaxial tests on sand, and proposed a hyperbolic model of a stress-strain relationship of sand after liquefaction. Zhang and Wang (2004) proposed a constitutive model which can evaluate small to large cyclic strains of saturated sand during the liquefaction process based on the Ramberg-Osgood model. Wang and Wang (2009) proposed a constitutive model which included the low intensive strength stage, superlinear strength recovery stage and sublinear strength recovery stage. Xu *et al*. (2007) proposed a constitutive model which was composed of three lines based on laboratory tests of post liquefaction deformation of sand. Obviously, the accuracy of segment-line models used to reflect the stress-strain relationship of soil after liquefaction is not very high. The hyperbolic model cannot reflect the sublinear strength recovery stage of soil or the flow stage of soil under static loads.

The fine sand that mostly contains flake-shaped particles is widely distributed over the middle and lower reaches of Yangtze River. Its mineral composition is mainly mica and other deep colored mineral weathering. And, the engineering characteristics of the flake-shaped sand are different from quartz sand. Academician Zhou (1999) called it Nanjing sand. Chen *et al*. (2003) indicated that the flake-shaped particles have a greater effect on the liquefaction characteristics of the sand. Systematic research of the dynamic characteristics of Nanjing fine sand have been conducted by Chen and

Correspondence to: Chen Guoxing, Institute of Geotechnical Engineering, Nanjing University of Technology, Nanjing 210009, China
Tel: +86-25-83239595
E-mail: gxc6307@126.com
[†]PhD Candidate; [‡]Professor

Received December 2, 2010; **Accepted** May 5, 2011

Liu (2004; 2009), Chen and Pan (2010), Wang *et al.* (2010), including the threshold shear strain, the dynamic shear modulus and damping ratio, the increase and dissipation model of pore water pressure, the mode of seismic settlement and seismic damage. All of these further confirmed that there are remarkable differences between the dynamic characteristics of Nanjing fine sand and quartz sand. However, there is little research on the large post-liquefaction deformation of saturated Nanjing sand.

The stress-strain responses and the characteristics of excess pore water pressure after liquefaction were studied based on the laboratory test results. A constitutive model of stress-strain responses and a dissipation model of excess pore water pressure were established, and the influence of relative densities and confining pressure on the characteristics of liquefied soil were studied.

2 Brief introduction of tests

2.1 Test equipment

The hollow cylinder torsional apparatus employed in this study can impose an axial load W, torque M_T, external cell pressure P_e as well as inner cell pressure P_i on the specimen simultaneously and control four of them individually, as shown in Fig. 1.

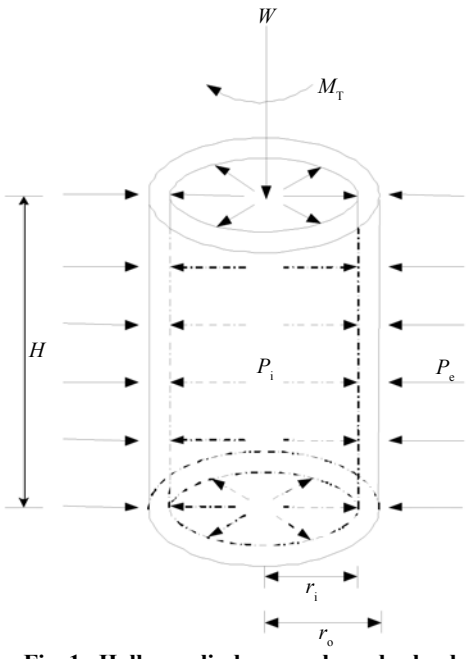

Fig. 1 Hollow cylinder sample under loads

Figure 2 shows the stress state of the hollow cylinder element. The shear stress $\tau_{z\theta}$ is induced by torque M_T, both the circumferential stress σ_θ and the radial stress σ_r are induced by external cell pressure P_e and inner cell pressure P_i, and the axial stress σ_z is induced by axial loads W, P_e and P_i. The radial stress σ_r is a principal stress because there is no shear stress on the inner and external walls of the specimen.

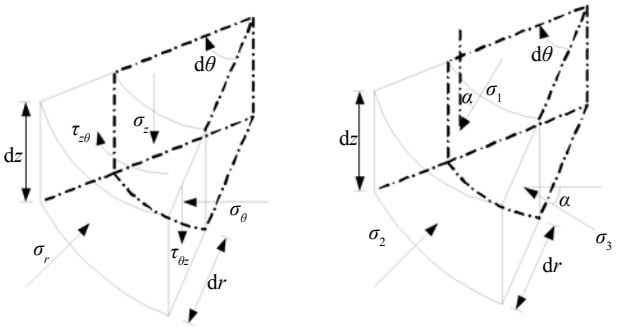

Fig. 2 Stress state of hollow cylinder sample

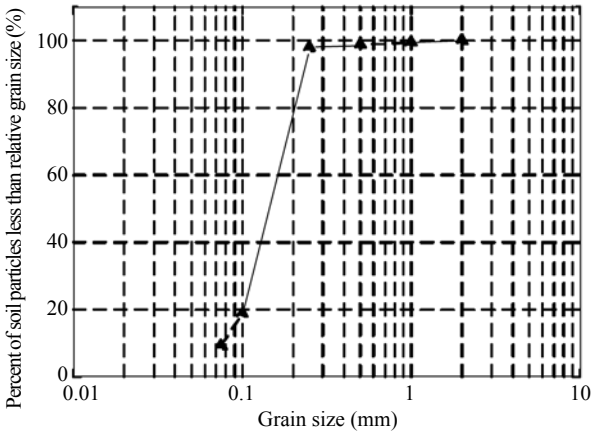

Fig. 3 Grain size distribution curve of Nanjing fine sand

2.2 Test materials

The tests were carried out on the samples of Nanjing saturated fine sand and the grain-size distribution is given in Fig. 3. The basic physical properties of such sand were measured. Its specific gravity is $G_s = 2.70$, natural dry density is $\rho_d = 1.49$, and maximum and minimum void ratios are e_{max}=1.14 and $e_{min} = 0.62$, respectively.

2.3 Test scheme

The inner and outer radii of the cylindrical samples are 30 mm and 50 mm and the height of the samples is 200 mm. The dry deposition method was employed in the sample preparation. Oven-dried sand was weighed and poured into the hollow space between two molds with a brush and a funnel in eight layers. Each interface was de-aired when compacted to the corresponding height to ensure a close contact of each layer. When filling of dry sand was finished, CO_2 gas was flowed to replace the air. The specimen was subsequently filled with de-aired water which had been circulated for about 30 min. Back pressure was then applied incrementally up to approximately 300 kPa to saturate the specimen. Pore water pressure parameter B of all the prepared samples was required to gain a value over 0.98. Cyclic loading was imposed on the specimens after the consolidation stage in order to liquefy the specimens, then static

loading was imposed on the liquefied specimens at a certain strain speed, as shown in Fig. 4.

The influence of relative densities and confining pressure on the characteristics of liquefied soil were studied in this research: (1) confining pressure σ_0' equaled 100, 200, 300 kPa, respectively, and (2) relative densities D_r equaled 30%, 50%, 70%, respectively.

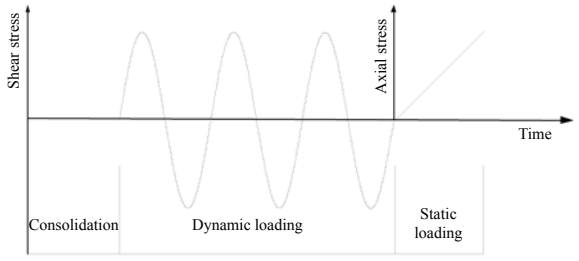

Fig. 4 Loading process in post-liquefaction tests of soil sample

3 Test results and analysis

Figures 5–7 shows the test results of the stress-strain relationship of Nanjing saturated fine sand after liquefaction under different confining pressures and relative densities, and Fig. 5 also shows the dissipation curve of pore water pressure. It can be found that the stress-strain relationship of liquefied sand is different from that under ordinary static triaxial tests. The stress-strain relationship of liquefied sand can be divided into three stages, ε_0 is the strain demarcation point of stage one and two, and ε_1 is the strain demarcation point of stage two and three.

In the first stage, the tangent modulus of sand increases from zero to a minimal value, the axial strain ε_a increases quickly, the deviator stress q almost equals zero, and the pore water pressure almost remains as the confining pressure. The sand almost presents as a fluid body and it cannot bear any shear stress. Thus, this stage is called the low intensive strength stage defined by Shamoto *et al*. (1997). It is because the effective stress of the liquefied sand almost equals zero, the specimen has a trend of vibro-compaction under the cyclic loading, and the water of the specimen is under the compression status. Then there is a trend of shear dilation in the specimen under the static loading, and the water of the specimen transforms from compression status to free state. In the transformation process, the effective stress almost maintains as zero, but the axial strain increases greatly.

In the second stage, the water of the specimen transforms to a free state entirely as the axial strain develops. The pore water pressure decreases quickly, and the effective stress increases fast, thus the strength of the specimen recovers gradually, and the stress-strain curve appears as upper concave.

The third stage can be divided into two small phases. The specimen is also under the state of shear dilation in the first small phase, and the deviator stress q increases continuously. However, the stress-strain curve becomes gentle, and it appears as an upper convex. The specimen is destroyed under the static loading, and it appears as a fluid body again; the stress-strain curve is a horizontal line.

Figure 6 shows the stress-strain curves of Nanjing saturated fine sand after liquefaction under different confining pressures σ_0' when relative densities D_r equals 50%. It can be found that: σ_0' has a significant effect on the stress-strain curves of liquefied sand. The values of ε_0 and ε_1 decrease as σ_0' increases, but the ultimate strength of sand increases with σ_0'.

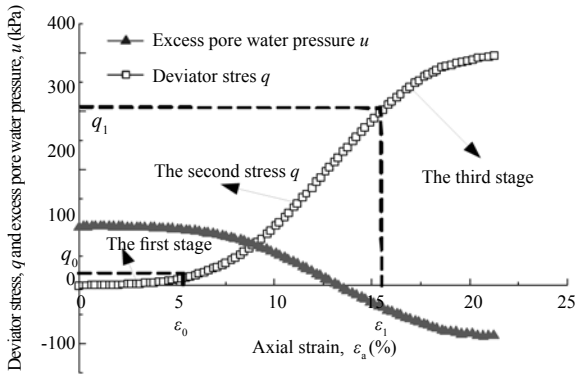

Fig. 5 Relationship between deviator stress q, excess pore water pressure u and axial strain ε_a when D_r = 50%, σ_0'=100 kPa

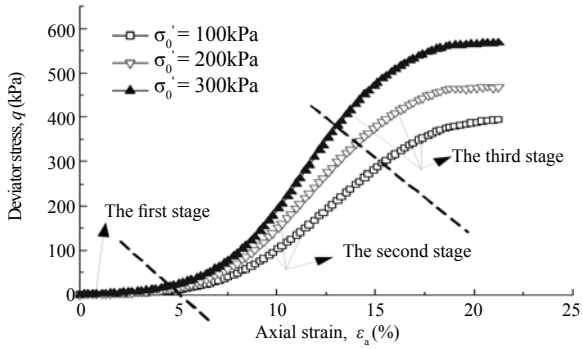

Fig. 6 Influence of σ_0' on the relationships between deviator stress q and axial strain ε_a

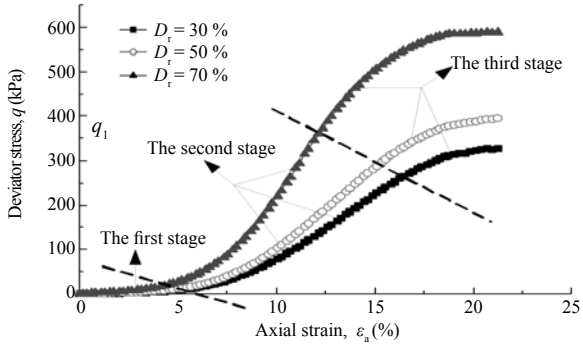

Fig. 7 Influence of D_r on the relationships between deviator stress q and axial strain ε_a

Figure 7 shows the stress-strain curves of Nanjing saturated fine sand after liquefaction under different relative densities D_r when confining pressures σ_0' equals 100 kPa. It can be found that: D_r has a significant effect on the stress-strain curves of liquefied sand. The values of ε_0 and ε_1 decrease as D_r increases, but the ultimate strength of sand increases with D_r.

4 Stress-strain relationship of liquefied saturated Nanjing fine sand

4.1 Mathematical model of stress-strain relationship

According to the characteristics of the stress-strain relationship of liquefied sand, a sigmoid curve can be used to fit the test data (see Fig. 8), its function expression is shown in Eq. (1).

$$q = \frac{a}{1 + b \times \mathrm{e}^{-k \cdot \varepsilon_a}} - \frac{a}{b+1} (k > 0) \tag{1}$$

where $\frac{ab}{b+1} = \lim_{\varepsilon_a \to +\infty} q$, set $\frac{ab}{b+1} = q_{\mathrm{ult}}$, q_{ult} is the ultimate value of deviator stress q.

Because the stress-strain curve of liquefied sand changes from upper concave to upper convex, there must be a inflection point, A, whose coordinate is $A(\varepsilon_x, a/2)$. The parameters *a, b, k* can be determined by Eq. (2).

$$\begin{cases} ab/(b+1) = q_{\mathrm{ult}} \\ b \cdot \mathrm{e}^{-k \cdot \varepsilon_x} = 1 \\ q''(\varepsilon_x) = 0 \end{cases} \tag{2}$$

Figures 9 and 10 show all the results fitted by Eq. (1), and the fitting parameters *a, b* and *k* are summarized in Table 1. The results show that the sigmoid curve can reflect the stress-strain relationship of liquefied saturated Nanjing fine sand.

Based on the results of Table 1, the fitting parameters *a, b* and *k* can be determined by relative densities D_r and effective confining pressures σ_0', as shown in Eq. (3).

$$\begin{cases} a = (322.300 + 0.854\sigma_0') \times (1.2077 - 2.356D_r + 3.882D_r^2) \\ b = (158.7 + 0.075\sigma_0') \times (1.9046 - 2.9913D_r + 2.364D_r^2) \\ k = (0.374 + 0.0003\sigma_0') \times (0.789 + 0.484D_r) \end{cases} \tag{3}$$

4.2 Verification of the constitutive model

Another two tests were used to verify the applicability of the constitutive model, they were $D_r = 0.4$, σ_0'=150 kPa and $D_r = 0.6$, σ_0'=250 kPa. The tested and predicted curves of stress-strain responses are shown in Fig. 11. It can be found that the results of the experiment generally agree with the predicted analyses. This means that the constitutive model has a good applicability.

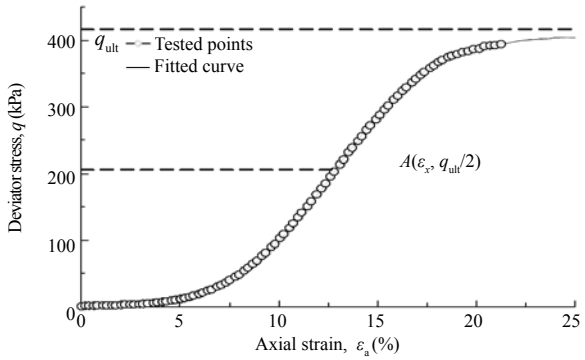

Fig. 8 Comparison of tested and predicted curves of stress-strain responses

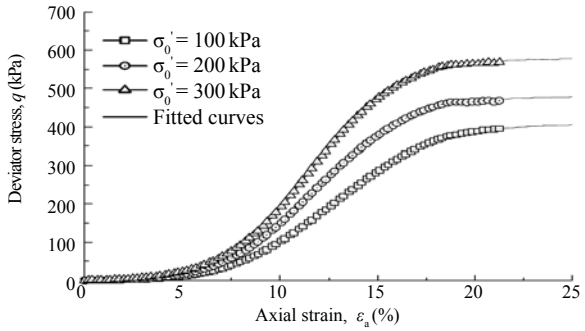

Fig. 9 Fitted results of stress-strain responses under different initial effective confining pressures

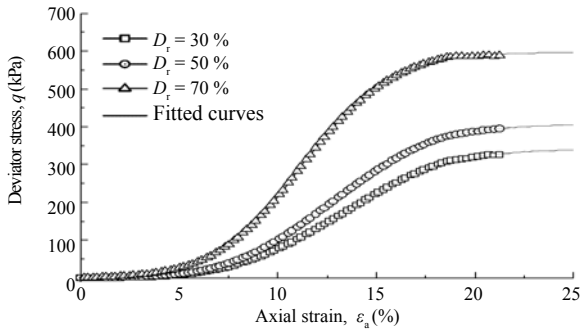

Fig. 10 Fitted results of stress-strain responses under different relative densities

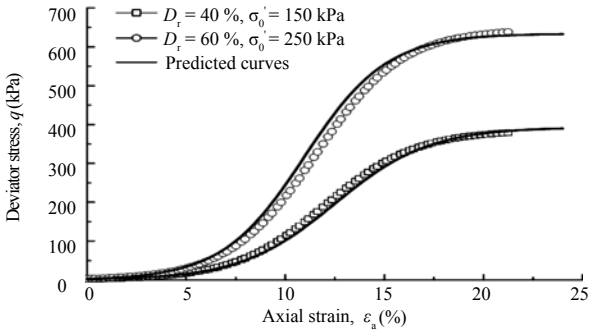

Fig. 11 Comparison of test and predicted curves of stress-strain responses of verifying tests

Table 1 Fitting values of parameters under different test conditions

σ_0' (kPa)	D_r = 30 %			D_r = 50 %			D_r = 70 %		
	a (kPa)	*b*	*k*	*a* (kPa)	*b*	*k*	*a* (kPa)	*b*	*k*
100	351.745	202.401	0.378	412.558	165.905	0.398	602.489	160.783	0.455
200				483.325	174.230	0.425			
300				583.276	180.870	0.448			

5 Dissipation model of pore water pressure of liquefied saturated Nanjing fine sand

5.1 Establishment of the dissipation model of pore water pressure

Figures 12 and 13 show the relationship between excess pore water pressure u and axial strain ε_a of liquefied saturated Nanjing fine sand. It can be found that, like the stress-strain relationship, the dissipation process of u can also be divided into three stages, and the demarcation points of each stage are basically in accordance with those of the stress-strain relationship.

Based on the research on the test data, it was found that there is a good linear relationship between normalized pore water pressure and deviator stress of liquefied saturated Nanjing fine sand, as shown in Eq. (4).

$$\frac{u}{\sigma_0'} = \frac{c}{\sigma_0'} + d\left(\frac{q}{\sigma_0'}\right) \tag{4}$$

where $c = \lim_{q \to 0} u$, thus parameter c means the pore water pressure corresponding to the initial moment of the static loading imposed on the liquefied sand. Because all the tests in this paper were made under isotropic consolidation, the pore water pressure under the dynamic loading can reach the initial effective confining pressure σ_0'. This means that $c = \sigma_0'$, thus, Eq. (4) can be rewritten as:

$$\frac{u}{\sigma_0'} = 1 + d\left(\frac{q}{\sigma_0'}\right) \tag{5}$$

Figures 14 and 15 show all the results fitted by Eq. (5), and the fitting parameter d is summarized in Table 2.

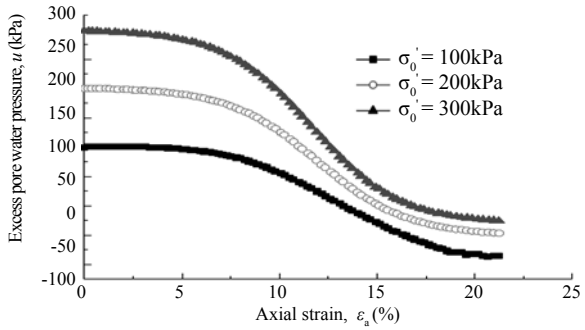

Fig. 12 Influence of σ_0' on the relationship between excess pore water pressure u and axial strain ε_a

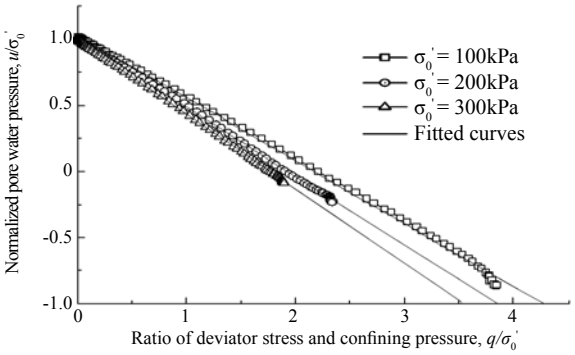

Fig. 14 Fitted results of normalized pore water pressure under different confining pressures

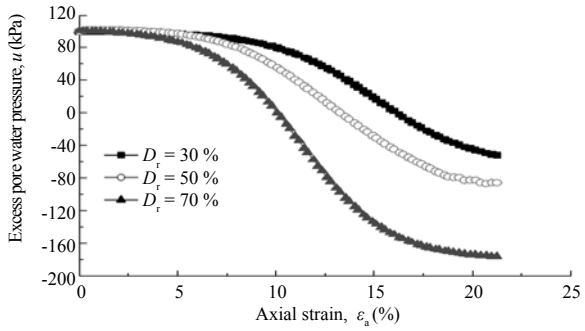

Fig. 13 Influence of D_r on the relationship between excess pore water pressure u and axial strain ε_a

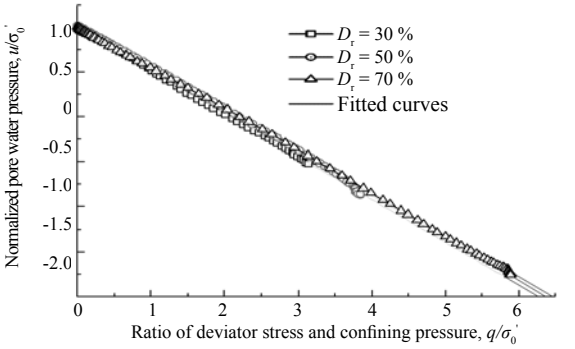

Fig. 15 Fitted results of normalized pore water pressure under different relative densities

Table 2 Value of parameter *d* under different test conditions

σ_0'(kPa)	D_r = 30%	D_r = 50%	D_r = 70%
100	-0.479	-0.477	-0.466
200		-0.521	
300		-0.564	

It can be found that the fitting parameter *d* (the slope of the line) is independent on the relative density, and the relationship between parameter *d* and effective confining pressure σ_0' can be expressed as Eq. (6).

$$d = -0.4336 - 0.0435 \times (\frac{\sigma_0'}{P_a}) \quad (6)$$

where P_a is the standard atmospheric pressure, P_a = 100 kPa.

5.2 Verification of the dissipation model of pore water pressure

Another two tests were used to verify the applicability of the dissipation model of pore water pressure: they were D_r = 0.4, σ_0'=150 kPa and D_r = 0.6, σ_0'=250 kPa. The tested and predicted curves of normalized pore water pressure and deviator stress are shown in Fig.16. It can be found that the results of the experiment generally agree with the predicted analyses. This means that the dissipation model of pore water pressure has a good applicability.

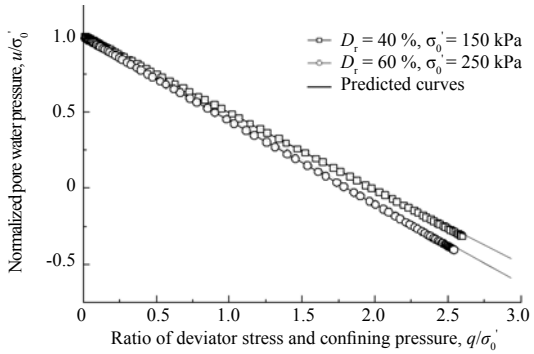

Fig. 16 Comparison of tested and predicted curves of normalized pore water pressure

6 Conclusions

Through static loading tests on the liquefied saturated Nanjing fine sand, it can be found that:

(1) The stress-strain responses and the dissipation process of pore water pressure of liquefied saturated Nanjing fine sand can all be divided into three stages, and each demarcation point is basically identical.

(2) The relationship between deviatoric stress and axial strain presents as a sigmoid curve. There is a good linearity relationship between normalized pore water pressure and deviatoric stress. And, the verification tests show that the experimental results generally agree with the predicted analyses for the two models.

(3) The relative densities and effective confining pressure all have a significant influence on the stress-strain responses of liquefied saturated Nanjing fine sand. However, the dissipation model of excess pore water pressure is only affected by the effective confining pressure.

References

Bartlett SF and Youd TL (1995), "Empirical Prediction of Liquefaction Induced Later Spread," *J. of Geotech Engrg*, ASCE, **121**(4): 316–329.

Chen GX and Liu XZ (2004), "Testing Study on Ratio of Dynamic Shear Moduli and Ratio of Damping for Deposited Soils in Nanjing and Its Neighboring Areas," *Chinese Journal of Rock Mechanics and Engineering*, **23**(8): 1403–1410. (in Chinese)

Chen GX and Liu XZ (2009), "Undrained Cyclic Behaviors of Nanjing Flake-shaped Fine Sand Under Cyclic Loading," *Chinese Journal of Geotechnical Engineering*, **31**(10): 1498–1504. (in Chinese)

Chen GX and Pan H (2010), "Effect of Initial Stress Conditions on the Threshold Shear Strain of Nanjing's Saturated Fine Sand," *Earthquake Research in China*. **24**(1):128–136.

Chen WH, Sun M and Liu ML (2003), "Characters of Schistose Structure of Nanjing's Sand and Seismic Liquefaction of Subsoil of A Metro Section," *Rock and Soil Mechanics*, **24**(5): 755–758. (in Chinese)

Hamada M, Isoyama R and Wakamatsu K (1996), "Liquefaction-induced Ground Displacement and Its Related Damage to Lifeline Facilities," *Soils and Foundations*, **SI**: 81–97.

Hamada M, Towhata I, Yasuda S and Isoyama R (1987), "Study on Permanent Ground Displacements Induced by Seismic Liquefaction," *Computers and Geotechnics*, **4**(4): 197–220.

Hamada M, Yasuda S and Isoyama R (1986), "Observation of Permanent Displacements Induced by Soil Liquefaction," *Proc JSCE*, **3**(6): 211–220.

Ishihara K and Yoshimine M (1992), "Evaluation of Settlements in Sand Deposits Following Liquefaction During Earthquakes," *Soils and Foundations*, **32**(1), 173–188.

Liu HL, Zhou YD and Gao YF (2002), "Study on the Behavior of Large Ground Displacement of Sand Due to Seismic Liquefaction," *Chinese Journal of Geotechnical Engineering*, **24**(2): 142–146. (in Chinese)

Shamoto Y, Zhang JM and Goto S (1997), "Mechanism of Large Post-liquefaction Deformation in Saturated Sands," *Soils and Foundations*, **37**(2): 71–80.

Tohno I and Shamoto Y (1985), "Liquefaction Damage to the Ground During the 1983 Nihonkai-Chubu Earthquake in Akita Prefecture," *Natural Disaster Science*, **7**(2): 67–93.

Tohno I and Shamoto Y (1986), "Liquefaction Damage to the Ground During the 1983 Nihonkai-Chubu

Earthquake in Aomori Prefecture," *Natural Disaster Science*, **8**(1): 85–116.

Tokimatsu K and Seed HB (1987), "Evaluation of Settlements in Sands Due to Earthquake Shaking," *Journal of the Geotechnical Engineering Division*, ASCE, **113**(8): 861–878.

Towhata I, Sasaki Y, Tokida K, Matsuoka H, Tamari Y and Yamada K (1992), "Prediction of Permanent Displacement of Liquefied Ground by Means of Minimum Energy Principle," *Soils and Foundations*, **32**(3): 97–116.

Wang BH Chen GX and Jin Dandan (2010), "Pore Water Pressure Increment Model for Saturated Nanjing Fine Sand Subjected to Cyclic Loading," *Earthquake Engineering and Engineering Vibration*, **9**(4): 569–576.

Wang YL and Wang Y (2009), "Experimental Study on Strength and Deformation Characteristics of Saturated Sand After Liquefaction," *Shuili Xuebao*, **39**(6): 667–672. (in Chinese)

Xu B, Kong XJ and Zou DG (2007), "Laboratory Study on Behavior of Static Properties of Saturated Sand-gravel After Liquefaction," *Chinese Journal of Geotechnical Engineering*, **29**(1): 103–106. (in Chinese)

Yasuda S, Yoshida N and Masuda T (1995), "Stress-strain Relationship of Liquefaction Sands," *Earthquake Geotechnical Engineering*, Rotterdam: Balkema, pp. 811–816.

Zhang JM and Wang G (2004), "A Constitutive Model for Evaluating Small to Large Cyclic Strains of Saturated Sand During Liquefaction Process," *Chinese Journal of Geotechnical Engineering*, **26**(4): 546–552.

Zhou J (1999), "Some Cases in Geotechnical Engineering," *Chinese Journal of Geotechnical Engineering*, **21**(1): 2–8. (in Chinese)